LASER INTERFEROMETER GRAVITATIONAL WAVE OBSERVATORY
- LIGO -
CALIFORNIA INSTITUTE OF TECHNOLOGY
MASSACHUSETTS INSTITUTE OF TECHNOLOGY

Technical Note **LIGO-T1800296–v1** 2018/09/28

Constructing a Balanced Homodyne Detector for Low Quantum Noise Gravitational Wave Interferometry

John Martyn
Mentors: Andrew Wade, Kevin Kuns, Aaron Markowitz, Rana Adhikari

California Institute of Technology
LIGO Project, MS 18-34
Pasadena, CA 91125
Phone (626) 395-2129
Fax (626) 304-9834
E-mail: info@ligo.caltech.edu

Massachusetts Institute of Technology
LIGO Project, Room NW22-295
Cambridge, MA 02139
Phone (617) 253-4824
Fax (617) 253-7014
E-mail: info@ligo.mit.edu

LIGO Hanford Observatory
Route 10, Mile Marker 2
Richland, WA 99352
Phone (509) 372-8106
Fax (509) 372-8137
E-mail: info@ligo.caltech.edu

LIGO Livingston Observatory
19100 LIGO Lane
Livingston, LA 70754
Phone (225) 686-3100
Fax (225) 686-7189
E-mail: info@ligo.caltech.edu

http://www.ligo.caltech.edu/

Abstract

As gravitational wave interferometers increase their sensitivity, sources of quantum noise dominate over classical noise sources. Further reduction of noise requires gravitational wave observatories to use non-classical, squeezed states of light, in which the quantum noise of one quadrature is decreased while that of another is increased. A balanced homodyne detector can measure an arbitrary quadrature of light by mixing a weak signal with a strong source of light. Balanced homodyne readout can be used to perform precise interferometry with squeezed light, and will be incorporated into LIGO in its A+ upgrade. As squeezed states of light are crucial to future gravitational wave physics, numerous research labs seek to perform experiments with balanced homodyne detectors. Therefore, we aim to construct the optical components and readout electronics for a balanced homodyne detector that may be used in various LIGO research labs performing experiments with non-classical light.

Contents

1 Introduction and Background

1.1 Noise in Gravitational Wave Observatories

Achieving more efficient detection of gravitational radiation is a goal of contemporary experimental physics, as it will enable novel tests of general relativity and provide information on astronomical bodies that are difficult to observe through the electromagnetic spectrum. The gravitational waves (GWs) that encompass this radiation are described by oscillatory perturbations to a background spacetime metric and manifest themselves physically by altering displacements in spacetime. Current GW observatories, such as LIGO, use high precision laser interferometry to detect GW strains on the order of 10^{-21}. To conduct the incredibly precise measurements necessary to observe GWs, LIGO uses a large Michelson interferometer furnished with Fabry-Perot cavities and power recycling mirrors.

Despite their intricate designs, interferometric GW detectors are subject to various sources of noise that limit their resolution. Some noise sources, such as seismic noise or electronic noise, can be combated by numerous techniques, including vibration isolation systems and use of low noise electronics. However, as gravitational wave interferometers increase their sensitivity, classical noise is superseded by quantum noise, a noise source that owes its existence to the Heisenberg uncertainty principle and quantum fluctuations. For instance, in quantum electrodynamics (QED), the quantized electromagnetic field reveals the discrete photon nature of light, introducing shot noise and radiation pressure noise into the interferometer. Sources of quantum noise dictate that the sensitivity of classical GW interferometers is bounded below by the Standard Quantum Limit (SQL). For example, in a GW interferometer with arm lengths L, test masses of mass m, and detecting a GW of frequency Ω, the noise spectral density of the GW strain, h, is bounded below by [9]

$$S_h^{\mathrm{SQL}}(\Omega) = \frac{2\hbar}{m\Omega^2 L^2}. \tag{1}$$

In general, the SQL will differ depending on the precise interferometric setup, but the limitations that it conveys remain the same.

1.2 Balanced Homodyne Detection and Squeezed Light

Interestingly, it turns out that the SQL only applies to interferometers when the sources of noise are uncorrelated, as they are classically [2]. Despite its counterintuitive name, the SQL can be surpassed by cleverly constructed interferometers that take into account quantum mechanics and correlated noise.

One such method of beating the SQL utilizes squeezed light and balanced homodyne detection. A balanced homodyne detector (BHD) is composed of two photodiodes, a 50/50 beam splitter, and two sources of light: the signal and the local oscillator. An image of a BHD setup is displayed in Figure 1. The signal is the light that encodes the desired information, and the local oscillator (LO) is a stable source of light with its carrier frequency equal to that of the signal. In an interferometer, the LO can be picked off from the main signal beam before it reaches the main interferometer. In balanced homodyne detection, these two sources of light are mixed and sent through the beam splitter, while two photodiodes

measure the photocurrents induced by the beams emerging from the beam splitter. One can then measure and analyze these photocurrents, from which information about the signal can be extracted.

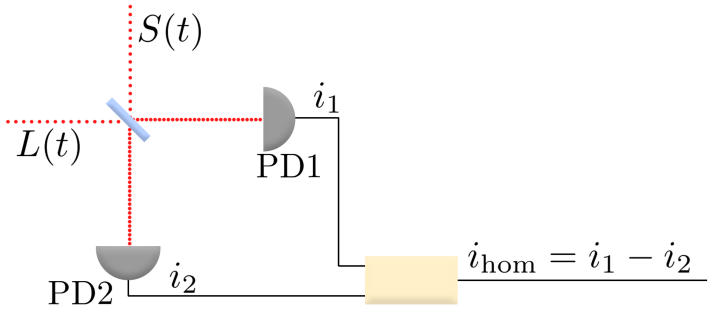

Figure 1: A standard BHD setup. $S(t)$ is the signal, and $L(t)$ is the local oscillator. The photodiodes, PD1 and PD2, produce photocurrents i_1 and i_2, respectively. The homodyne current, $i_{\rm hom}$, is the difference between these currents.

Following the analysis presented in [4], we can describe this procedure mathematically. Let the electric fields of the signal and LO have quadratures $S_{c,s}(t)$ and $L_{c,s}(t)$, respectively, and carrier frequency ω:

$$S(t) = S_c(t)\cos(\omega t) + S_s(t)\sin(\omega t), \qquad L(t) = L_c(t)\cos(\omega t) + L_s(t)\sin(\omega t). \tag{2}$$

Inevitably, the quadratures will contain noise in the form of quantum noise or other noise sources. Denoting these noises by $s_{c,s}(t)$ and $l_{c,s}(t)$, respectively, the quadratures can be decomposed as

$$\begin{aligned} S_{c,s}(t) &= \text{signal} + \text{noise} = S^0_{c,s}(t) + s_{c,s}(t) \\ L_{c,s}(t) &= \text{classical field} + \text{noise} = L^0_{c,s}(t) + l_{c,s}(t). \end{aligned} \tag{3}$$

Since the LO is under the experimentalist's control, we will impose on it a phase shift, ϕ_{LO} and assume that it is more intense than the other fields in this scenario: $L^0_c(t) = L_0\cos(\phi_{LO})$, $L^0_s(t) = L_0\sin(\phi_{LO})$ and $L_0 \gg S^0_{c,s}, s_{c,s}, l_{c,s}$. Under these conditions, it is straightforward to calculate the ideal photocurrents induced at the two photodiodes, which we denote by i_1 and i_2. However, in balanced homodyne readout, one chooses not to measure these currents, but instead measures their difference: $i_{\rm hom} = i_1 - i_2$. To first order in $S^0_{c,s}$, $s_{c,s}$, and $l_{c,s}$, this is given by [4]

$$i_{\rm hom} \propto L_0((S^0_c + s_c)\cos(\phi_{LO}) + (S^0_s + s_s)\sin(\phi_{LO})). \tag{4}$$

Evidently, this expression is independent of $l_{c,s}$, so noise from the LO does not factor into measurements of $i_{\rm hom}$. In addition, Eq. (4) indicates that, by varying the homodyne angle, ϕ_{LO}, and measuring $i_{\rm hom}$, one can determine the signal's quadratures and arbitrary linear combinations of them, with a precision limited only by the noise of the signal. Therefore, if one uses a signal with low quadrature noise, such as squeezed light, BHD provides exceptionally accurate quadrature measurements.

Squeezed light is a quantum state of light described through the formalism of quantum mechanics and QED. In QED, the electric field of a beam of light can be described by amplitude and phase quadrature operators, $\hat{X}_1$ and $\hat{X}_2$, respectively. By the canonical commutation relations of QED, the quadrature operators do not commute, and therefore obey an uncertainty principle, wherein the product of their uncertainties cannot decrease below 1: $\sigma_{\hat{X}_1}\sigma_{\hat{X}_2} \geq 1$. The quadrature uncertainties are therefore finite, which limits the ability to use classical light for precision interferometry. To counter this effect, one can instead use squeezed states of light, in which one quadrature uncertainty is decreased while the other is increased, such that the uncertainty principle is still satisfied. Balanced homodyne readout can then be used to measure the quadrature with reduced noise and obtain low noise measurements.

Finally, we note that the cancellation of the LO noise in Eq. (4) requires that the two paths in the BHD be identical. If there is an imbalance in the paths, LO noise can leak into i_{hom} and spoil the balanced homodyne readout. Such an imbalance may arise from a beam splitter that is not perfectly 50/50, photodiodes with different responsivities, or inequivalent readout electronics. To correct for an imbalance, one introduces a relative gain, α, which is close to unity, and analyzes $i'_{\text{hom}} = i_1 - \alpha i_2$ instead. With a properly adjusted relative gain, the LO noise again cancels out.

1.3 GW Observatory Implications

Current gravitational wave observatories do not exploit balanced homodyne detection of this sort. Instead, these experiments use DC readout [3], in which a single photodetector measures the light output from the main interferometer's beam splitter. As shown in [4], DC readout schemes are affected by the noise in the LO, unlike ideal balanced homodyne readout. However, realistic balanced homodyne detectors are quite sensitive to noise if there is any imbalance in the apparatus. Fortunately, this issue can likely be mitigated by precisely constructing a BHD to meet certain low noise requirements. Moreover, DC readout schemes are not as effective as balanced homodyne readout at measuring arbitrary quadratures of light in an interferometer. Therefore, we believe that balanced homodyne detection will enable more precise interferometry in GW detectors than the current DC readout schemes do. In fact, LIGO plans to switch from DC readout to balanced homodyne readout in its A+ upgrade in the early 2020's.

In this project, we first discuss our approach to creating a BHD. We then analyze measurements taken with it, and discuss some potential improvements. We hope that further research into this technology will enable physicists to make great use of balanced homodyne detection and enhance GW observatories.

2 Approach

Our aim is to construct the components of a BHD that can be used for various LIGO experiments. This procedure can be broken into two major steps: assembling the optical setup and constructing the electronics. The optical setup consists of the beam splitter, the photodiodes, an optical isolator, mirrors, and beam dumps. The electronics are primarily

composed of transimpedance amplifiers, filters, and other circuits that process the signals from the photodiodes.

Moreover, we desire the BHD to be shot noise limited: the electronic noise in the BHD ought to be 10 dB less than the shot noise of the light, such that we can observe squeezed light with this device. We also aim to operate our BHD up to a frequency of roughly 2 MHz. These precise constraints and their implications are discussed further in the coming sections.

2.1 Optics

The optical setup used for our BHD is shown in Figure 2. In this configuration, I used a 1064 nm Nd:YAG laser producing a TEM_{00} Gaussian beam with a power of 1 mW. This laser can simulate the signal or the LO, and provides a method to test the BHD. Before the laser beam reaches the BHD, it first passes through wave plates, a Faraday isolator, and a polarizing beam splitter (PBS). The first quarter-waveplate linearly polarizes the light emitted from the laser, and the subsequent half-waveplate aligns its polarization with the polarization axis of the Faraday isolator. Next, the Faraday isolator ensures that light is transmitted only in the forward direction, reducing interference between the back-scattered light and the beam. Finally, another half-waveplate alters the polarization of the output light, and the following PBS extinguishes one polarization by sending it to a beam dump, while allowing the other polarization to pass through to the next stage. By tweaking the fast axis of the final half-waveplate, we can alter the polarization of the light before it reaches the PBS. When combined with the PBS, this allows us to control the power of the light entering the BHD. In addition, four more beam dumps were included in order to capture scattered and reflected light produced by this setup, which would otherwise interfere with the light in the BHD. After this stage, the beam is steered with steering mirrors and sent to the beam splitter of the BHD. The two outgoing beams then impinge upon the photodiodes, from which photocurrents are measured.

For the BHD photodiodes, we incorporated two Laser Components InGaAs PIN photodiodes (part number: IG17X3000G1i), one of which is pictured in Figure 3. We characterized the response of these photodiodes by measuring their optical transfer function when connected to the basic transimpedance amplifier circuit shown on the left in Figure 4. The right image in Figure 4 displays a Bode plot of our measurements over the modulation frequency range of 30 kHz-30 MHz for incident laser powers of 69 μW and 95 μW. Since the 69 μW and 95 μW plots line up well, the photodiode's response is independent of power of the incident light. In addition, the photodiodes display a relatively stable gain of roughly $10^4 \frac{\text{V}}{\text{A}}$, until reaching a roll off frequency around 300 kHz. Since we are interested in signals up to 2 MHz, these photodiodes are sufficient for our purposes.

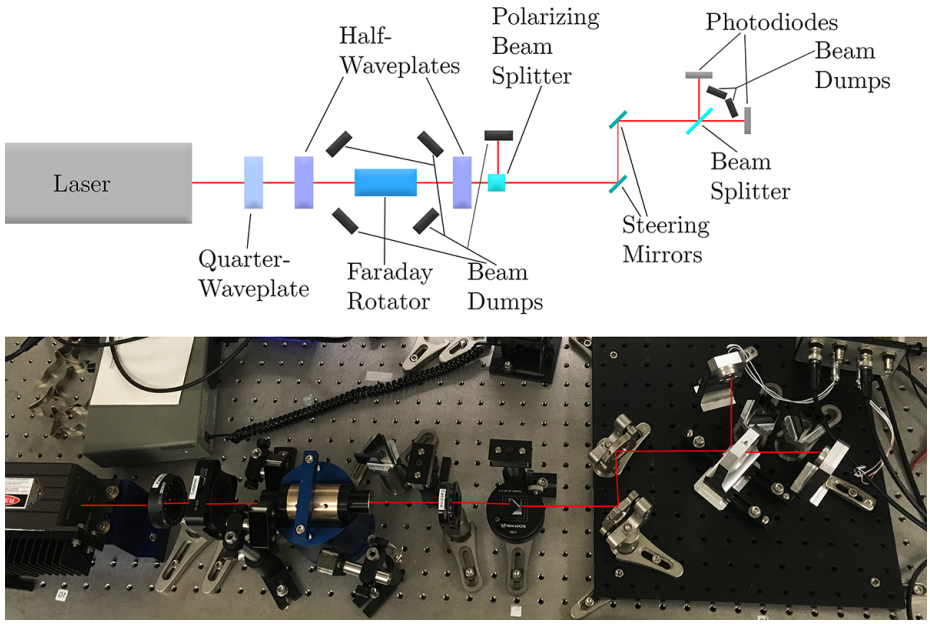

Figure 2: **Top**: A cartoon of the optical configuration used in the BHD. **Bottom**: An image of the optical configuration.

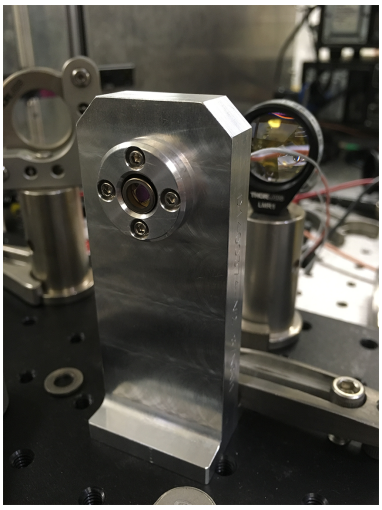

Figure 3: One of the Laser Components InGaAs PIN photodiodes used in the BHD.

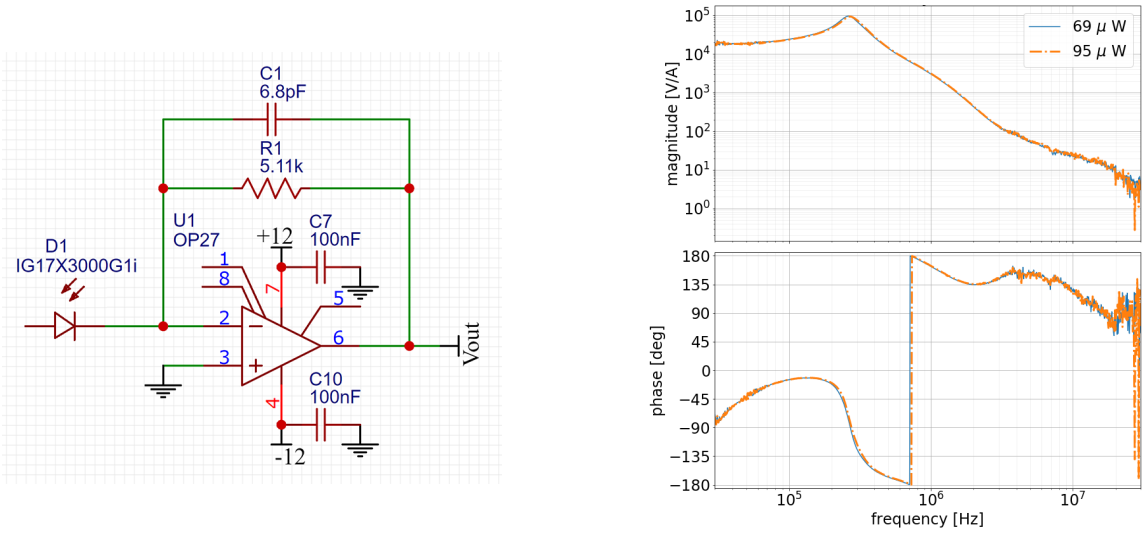

Figure 4: **Left**: The simple transimpedance amplifier circuit used to characterize the photodiodes. **Right**: Bode plot of the measured optical transfer function of the photodiode connected to the transimpedance amplifier over the frequency range 30 kHz - 30 MHz for incident light powers of 69 μW and 95 μW.

2.2 Electronics

The electronics in the BHD are used to process and readout the signals from the photodiodes. The circuits must amplify the signals from the photodiodes without significantly increasing their noise. Specifically, in order to observe squeezed light with our BHD, we desire its electronic noise to be at least 10 dB less than the shot noise of the light over a bandwidth of at least 10 kHz. After amplification and processing, the signals are sent to an analog-to-digital converter (ADC), which is used to perform digital subtraction and yield a measurement proportional to the homodyne current $i_{\text{hom}} = i_1 - i_2$.

To process the photocurrent from a photodiode, I used the circuit shown in Figure 5. On the left of this image is a transimpedance amplifier stage, labeled "Transimpedance Amplifier". This stage receives the current from the photodiode, denoted by I_p. Assuming that the op amp in this stage is ideal, no current flows through its inverting input, and so the photocurrent must flow through the resistor, R_1, and the feedback capacitor C_1. The feedback capacitor is placed in parallel with the resistor in order to provide compensation and stabilize the amplifier. Letting C_i denote the capacitance of the photodiode, an analysis of this situation reveals that the voltage output by this transimpedance amplifier is [11]

$$V = \frac{I_p R_1}{1 + \frac{1}{A_{OL}\beta}}, \quad \beta = \frac{1 + sR_1C_1}{1 + sR_1(C_1 + C_i)}, \quad s = i\omega, \tag{5}$$

where β is the feedback factor and A_{OL} is the open loop gain of the op amp. At low frequencies such that $A_{OL}\beta \gg 1$, this reduces to $V = I_p R_1$, and we say that the gain of the transimpedance amplifier is $R1$. For our circuit, the transimpedance amplifier stage has a gain of $R_1 = 5100\ \frac{\text{V}}{\text{A}}$. Therefore, the transimpedance amplifier stage in this circuit amplifies the photocurrent and sends its output to the three other stages of the circuit.

The top stage after the transimpedance amplifier, labeled "Differential Output", contains a buffer that cleans the output from the amplifier and ensures that this stage does not interfere with the others. This buffer, containing an op amp in its non-inverting configuration, produces a gain of

$$\text{Gain} = \frac{V_{\text{out}}}{V_{\text{in}}} = 1 + \frac{R_6}{R_7}. \tag{6}$$

Since $R_6 = 1000\Omega = R_7$ in this circuit, this buffer has a gain of 2. The rest of this stage is a differential amplifier that converts the output voltage from the buffer to a differential signal at the outputs denoted "LEMO1" and "LEMO2". We required a differential output so that the voltage produced by this circuit can be reliably sent to an analog-to-digital converter (ADC) that is roughly 30m away, in a separate lab where voltages are referenced to a possibly different ground. If we instead used a single ended output, the voltage produced by the circuit may be referenced to a ground that differs from that in the lab where the ADC is located, and hence our measurements conducted with the ADC would be inaccurate.

The middle stage, labeled "High Frequency", contains of an RC highpass filter. Such a filter has a cutoff frequency of

$$f_c = \frac{1}{2\pi R_5 C_3}, \tag{7}$$

below which frequency, signals are significantly diminished. In our case, the value of the cutoff frequency is 106 Hz. In addition, this stage contains a buffer amplifier with a gain of 10 that magnifies the signal and prevents interference between stages. The AC signal produced by this stage is sent to the output denoted "BNC1", which was used to analyze signals without interference from DC voltages or DC noise.

The final stage, "Low Frequency", contains an RC lowpass filter with a cutoff frequency of $\frac{1}{2\pi R_4 C_9} = 100$ kHz, followed by a unity gain buffer to reduce interference between stages. The processed voltage from this stage is sent to the "BNC2" output, from which we can examine low frequency and DC signals.

Two of these circuits (one for each photodiode) are encased in an aluminum box that protects them from external noise. The electronics in the box are shown in Figure 6. The front panel of the box contains ports for the photodiodes and the outputs discussed above, while the back panel has plugs from which the the readout electronics are powered. In our experiments, I powered the readout electronics with $\pm$15V from an SR560.

Finally, the processed signals from the electronics are sent to an analog-to-digital converter (ADC), from which data is collected to perform digital subtraction. This setup, along with the readout electronics and the BHD, are shown in Figure 7. We opted for digital subtraction instead of analog subtraction because the digital method provides more versatility. In particular, if there is an imbalance between the two photodiodes or their readout electronics, the photocurrent subtraction must be modified by a relative gain, α: $i_{\text{hom}'} = i_1 - \alpha i_2$. Since this procedure is easily implemented on a computer, digital subtraction is more robust against errors than its analog counterpart.

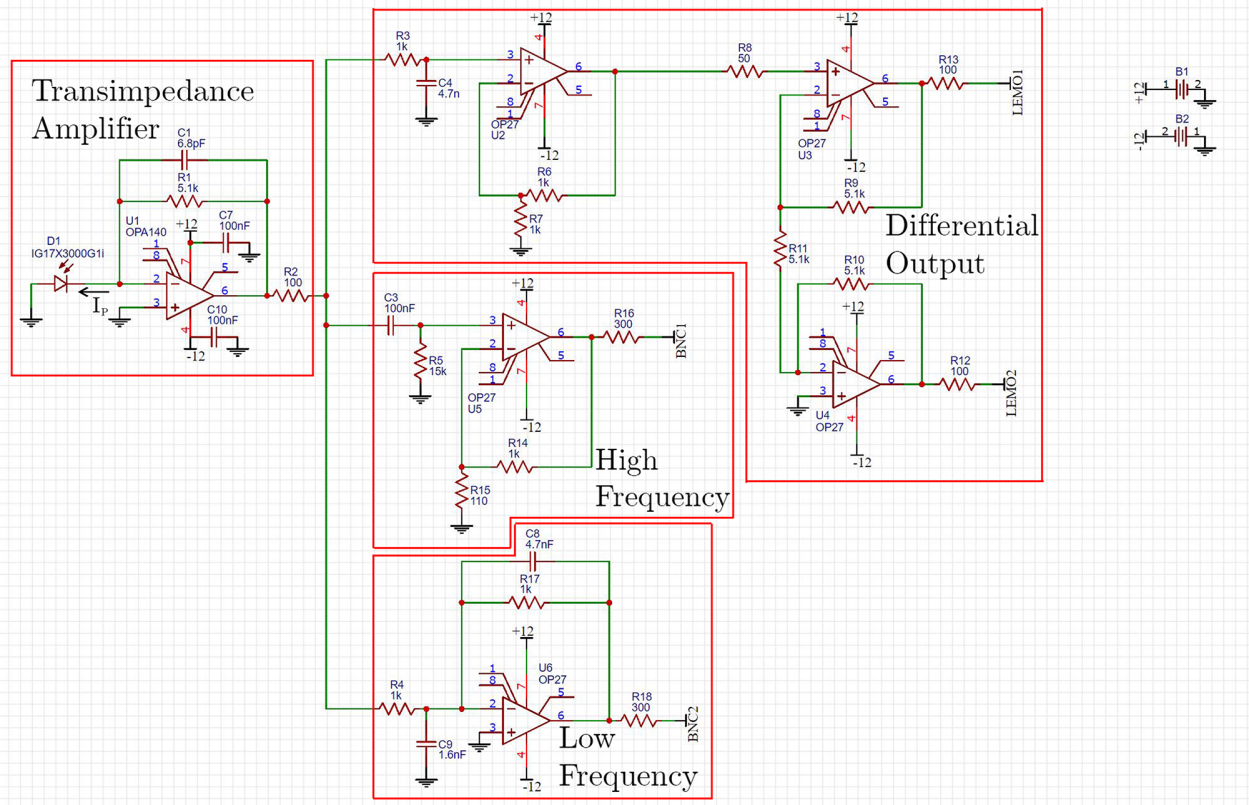

Figure 5: The readout circuit used to process signals from photodiodes.

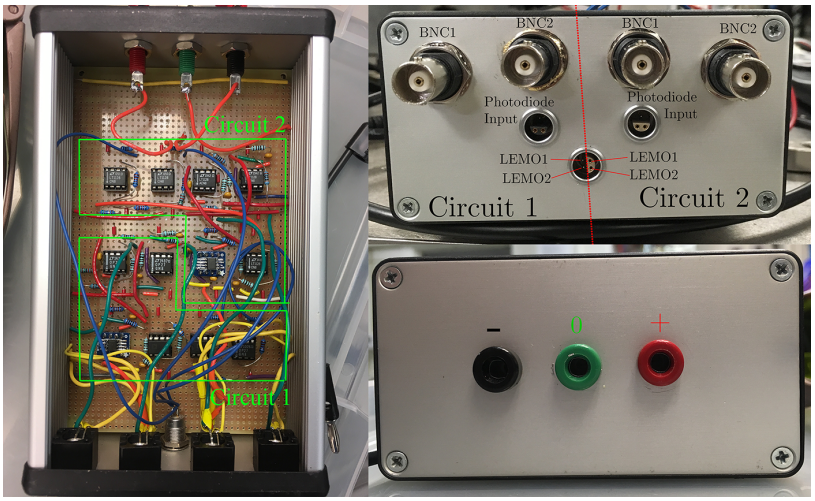

Figure 6: **Left:** The readout electronics (two circuits in total) in their box. **Top Right:** The front panel of the box with its inputs and outputs labeled. **Bottom Right:** The back panel of the box and the plugs used to power the electronics.

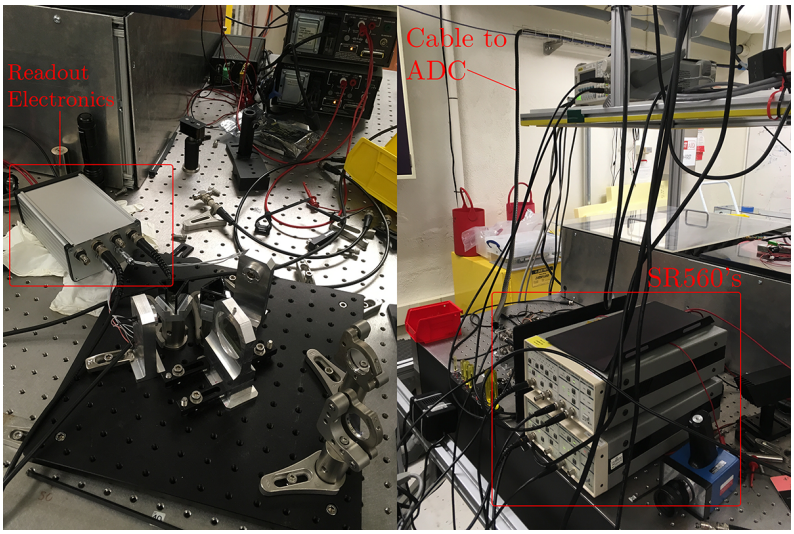

Figure 7: Setup of the BHD electronics, including the readout electronics, SR560's, and a cable to the ADC.

3 Results

3.1 SR785 Measurements

To demonstrate the functionality of our BHD, I injected into it an amplitude modulated laser beam with a frequency of 1.234 kHz, simulating a noisy LO. This is depicted schematically in Figure 8. The noise spectrum from this LO should display a peak at 1.234 kHz. If the BHD operates correctly, the noise spectrum of the homodyne signal should not display this peak when the signals are balanced.

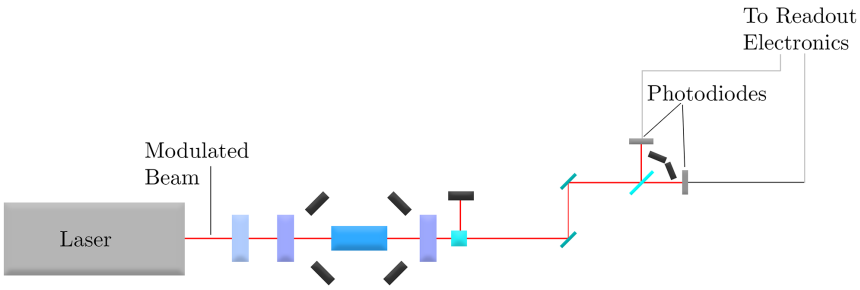

Figure 8: A cartoon of a modulated beam being injected into the BHD in order to simulate a noisy LO.

As our first test, I analyzed the outputs from the BNC2 ports and measured the noise of the homodyne signal with an SR785. The relative gain was adjusted by preamplifying the output signals with SR560's. Our measurements of input referred noise are displayed

in Figure 9. From this figure, we see that when the signals are unbalanced, there is a large spike in the noise spectrum at 1.234 kHz, corresponding to the noise in our LO. When the signals are balanced, this noise peak decreases significantly, and the spectrum displays a noise floor of roughly 700 $\frac{\text{pA}}{\sqrt{\text{Hz}}}$ in the kHz range. The vanishing of the peak demonstrates that the BHD has canceled out the LO noise. However, the balanced spectrum displays a plateau where the spike used to be, which shows that the cancellation is not perfect. Hence, we would ideally like to further eliminate the LO noise.

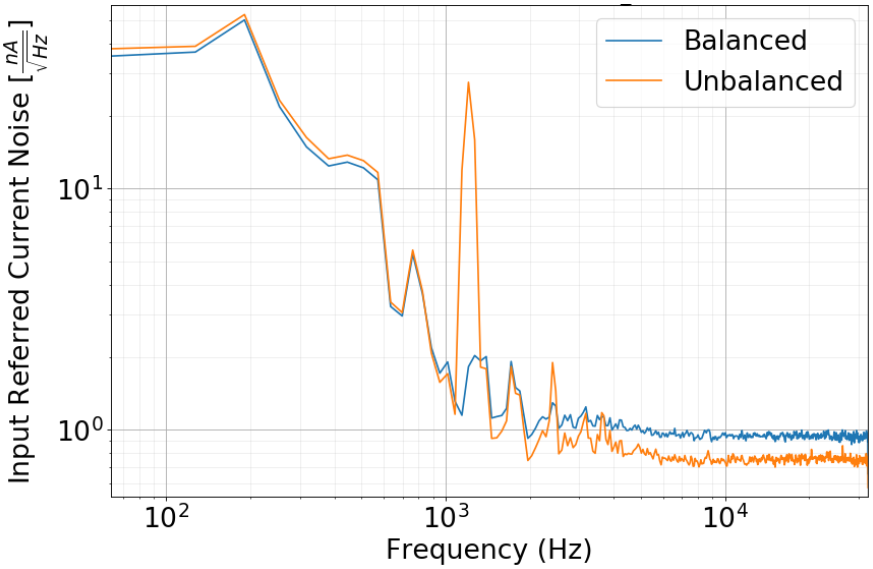

Figure 9: Unbalanced and balanced noise spectra of a 1.234 kHz signal measured with our BHD. Subtraction of signals was performed with an SR785 in these measurements.

3.2 ADC Measurements

I followed the above procedure an additional time, but now performed digital subtraction with ADC data and analyzed the noise on a computer. The resulting noise spectra are shown in Figure 10 under the label "Gain = 1", as no preamplification was applied to these signals. The unbalanced and balanced noise spectra are similar to those in Figure 9, both balanced noise spectra reaching a balanced noise floor of roughly 700 $\frac{\text{pA}}{\sqrt{\text{Hz}}}$ and displaying a plateau where the spike is in the unbalanced signal. Our digital subtraction mechanism thus works correctly, but we would still like to decrease the noise in our homodyne signal.

To reduce the noise further, I preamplified the BNC2 voltages with SR560's before sending the output to the ADC. The input referred noise spectra when the gain was set to 1000 are shown in Figure 10 under the label "Gain = 1000". The noise floor of the BHD electronics is also displayed under the label "Noise Floor". The balanced noise spectrum is relatively stable past 300 Hz, and attains a noise floor of roughly 20.2 $\frac{\text{pA}}{\sqrt{\text{Hz}}}$. This value is quite close to the noise floor of the BHD, which was measured at 12.6 $\frac{\text{pA}}{\sqrt{\text{Hz}}}$, indicating that our BHD performs quite well at eliminating LO noise and reducing the signal noise to a value on the order of the detector's noise floor. I should also note that there is a small peak in the balanced noise spectrum where the spike exists in the unbalanced spectrum. This peak is

less severe than the noise plateaus in the previous balanced noise spectra, but indicates that some LO noise is still leaking into the homodyne signal. As we desire no LO noise to affect our BHD measurements, improvements could be made to our BHD design.

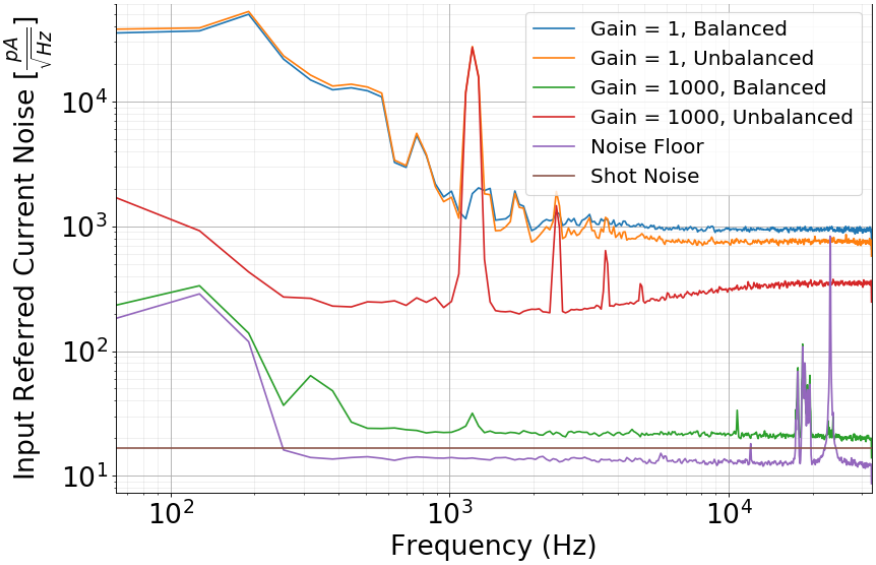

Figure 10: Unbalanced and balanced noise spectra of a 1.234 kHz signal measured with our BHD. In these measurements, subtraction was performed digitally with ADC data.

4 Future Work and Conclusions

4.1 Improvements

Clearly, our BHD is operative, but there exists ample room for improvement. In particular, we would like to decrease its noise to at least 10 dB less than the shot noise of the incident light. If we assume that our photodiodes have an ideal quantum efficiency of $\eta = 1$ and operate under 1064 nm light with a power of $P = 1$ mW, the shot noise is $\sqrt{2eI} = \sqrt{\frac{e^2 P}{5h\nu}} = 16.6 \frac{\text{pA}}{\sqrt{\text{Hz}}}$. This noise level is plotted as "Shot Noise" in Figure 10, from which it is evident that the BHD noise floor is slightly lower than shot noise, whereas the lowest balanced signal noise floor is slightly greater. Ideally, we would like to have our BHD noise be lower than the shot noise. A few changes should reduce the noise in the BHD and optimize its performance:

- Amplify the signal at a higher gain: The SR560's overloaded past a gain of 1000, which limited our noise reduction capabilities. Using a different low noise preamplifier that can produce higher gains without overloading should further decrease the noise of the BHD and the homodyne signal.
- Add bypass capacitors to the ±V pins on the op amps: Adding $\sim$ 100 nF capacitors from the ±V pins to ground will shield the op amps from high frequency noise in the power source. The impedance of a capacitor with capacitance C is $Z_c = \frac{1}{i\omega C}$. This

decreases as frequency increases, so high frequency voltages pass through the capacitors without significant attenuation. Hence by connecting bypass capacitors from ±V to ground, unwanted high frequency signals from the power source are sent to ground and eliminated.

- Replace OP27's with new op amps: The slew rate of an op amp is the maximum change in the input voltage per unit time that can be withstood before the output voltage becomes distorted. The slew rate quantifies the frequency range over which an op amp can operate properly. OP27's have a low slew rate and do not perform well at frequencies in the MHz range. In order to improve the high frequency performance of our BHD and decrease its noise, we should replace the OP27's with op amps that have a higher slew rate and a lower noise level, such as OP37's.

- Reverse bias the photodiodes: Applying a voltage to the cathodes of the photodiodes will increase their depletion regions and reduce their capacitances, making them more responsive to incident light. A reverse biased photodiode also has an electric field that helps move charges and generate current, overall rendering the signal more readable.

4.2 Conclusions

Our goal was to construct a balanced homodyne detector for use in LIGO experiments. The optical components and readout electronics assembled for the BHD are spelled out in Section 2. Ultimately, the results in Section 3 demonstrate that our BHD operates well and effectively eliminates LO noise. Nevertheless, refinements could be made in order improve its performance and applicability to experiments using non-classical light.

5 Acknowledgments

I am greatly indebted to my excellent mentors, Andrew Wade, Kevin Kuns, Aaron Markowitz, and Rana Adhikari. Together, their continual assistance and support guided me through this project and allowed me to accomplish my goals. I would also like to thank Johannes Eichholz, Tom Callister, Anchal Gupta, Gautam Venugopalan, Vinny Wagner, Koji Arai, Aidan Brooks, and Alan Weinstein for their help and friendliness throughout this program. Lastly, I am grateful for the Caltech SURF office, the LIGO SURF Program, the WAVE Fellows Program, and the NSBP Rouse Fellowship for providing me with this great summer research experience.

References

[1] A. I. Lvovsky, *Squeezed Light*. ArXiv e-prints (2016), arXiv:1401.4118v2 [quant-ph].

[2] M. Bassan, et. al, *Advanced Interferometers and the Search for Gravitational Waves*. (2014).

[3] K. Nakamura and M. Fujimoto *Double balanced homodyne detection*. ArXiv e-prints (2018), arXiv:1711.03713v2 [quant-ph].

[4] S. L. Danilishin and F. Y. Khalili, *Quantum Measurement Theory in Gravitational-Wave Detectors*. ArXiv e-prints (2012), arXiv:1203.1706v2 [quant-ph].

[5] H. Kogelnik and T. Li, *Laser Beams and Resonators*. Appl. Opt. **5**, 1550-1567 (1966)

[6] A. Zangwill, *Modern Electrodynamics*. (2013)

[7] S. M. Carroll, *Spacetime and Geometry: An Introduction to General Relativity*. (2004).

[8] H. Grote, et. al., *High power and ultra-low-noise photodetector for squeezed-light enhanced gravitational wave detectors*. Opt. Express, **24**, 20107-20118 (2016).

[9] H. Miao, *Exploring Macroscopic Quantum Mechanics in Optomechanical Devices*. (2012).

[10] H. W. Ott, *Noise Reduction Techniques in Electronic Systems*. (1988).

[11] J. G. Graeme, *Photodiode Amplifiers: Op Amp Solutions*. (1995).

[12] K. Thorne, *Ph237b: Gravitational Waves*. California Institute of Technology (2002).

[13] W. Ketterle, *8.422 Atomic and Optical Physics II*. Spring 2013. Massachusetts Institute of Technology: MIT OpenCourseWare, https://ocw.mit.edu. License: Creative Commons BY-NC-SA.